Physica Scripta. Vol. T41, 197–207, 1992.

Autoionization Versus Photoionization and Auger Decay of Physisorbed Molecular Adsorbates: Condensed Benzene on Cu(110)

T. Porwol, G. Dömötör and H.-J. Freund

Lehrstuhl für Physikalische Chemie 1, Ruhr-Universität Bochum, Universitätsstr. 150, 4630 Bochum, Federal Republic of Germany

R. Dudde

Fraunhofer Institut für Mikrostrukturtechnik, Margarete-Steiff-Weg 3, 2210 Itzehoe, Federal Republic of Germany

C.-M. Liegener

Institut für Physikalische und Theoretische Chemie, Universität Erlangen-Nürnberg, Egerlandstr. 3, 8520 Erlangen, Federal Republic of Germany

and

W. von Niessen

Institut für Physikalische und Theoretische Chemie, Technische Universität Braunschweig, Hans-Sommer-Str. 10, 3300 Braunschweig, Federal Republic of Germany

Received August 26, 1991; accepted October 14, 1991

Abstract

Autoionization spectra following core-to-bound excitation of benzene physisorbed on Cu(110) are presented. The inner valence region of the monocationic ion states, where the single particle picture is known to break down, dominates the spectrum. While autoionization and photoionization probe the same ion states transition intensities are different due to different selection rules. Especially the comparison between inner and outer valence region allows the identification of rather pronounced discrepancies. Core-to-continuum excitation leaves the molecule in a core ionized state which decays radiationless into outer valence double ionized states (Auger spectrum). Our interpretation is based on *ab initio* Green's function calculations for the inner and outer valence region followed by explicit calculations of the radiationless autoionization rates. In order to compare the transition rates for autoionization and Auger decay we have furthermore calculated the core–valence–valence Auger spectrum of benzene after C 1*s* excitation by the particle–particle Green's function method with subsequent calculation of the radiationless Auger rates. The simulated spectra after resonant and continuum excitation basically explain the experimental findings. The results show the usefulness of combining experimental and theoretical methods to study the radiationless decay even for large molecules.

1. Introduction

Photoelectron spectroscopy has become a valuable experimental tool in the study of the electronic structure of gaseous and solid molecules over the last decade. However, in the inner valence region the single particle picture is known to break down. That means instead of observing one single ion state a large amount of shake-up states is populated. In the gas phase a rich satellite structure is observable. The intensities due to second order effects are rather small and in solids and on surfaces they are hardly detectable due to the fact that secondary electron emission swamps the relatively low intensities. Within the last years a different approach has been used to study the inner valence region of molecules [1]: Dipol allowed core excitation into highly excited neutral states and subsequent autoionization into valence ionized states. Whereas the photoionization cross section is governed by the dipol operator the radiationless autoionization decay is governed by the coulomb operator. In a total energy diagram it can be seen that both spectroscopical methods basically populate the same final ion states [2]. Due to the $1/r$ dependence of the coulomb operator autoionization spectroscopy is a much more local probe of the electronic environment of the initially generated core hole as compared to photoionization. In the case of autoionization the transition matrix elements for the decay into single hole (1h) and two hole one particle (2h1p) states can present the same order of magnitude. This results in a high sensitivity for shake up states after core to bound excitation. The more traditional way of core excitation is the core to continuum excitation where the core excitated (N-1) electron state decays radiationless into double ionized final states. The Auger decay has been subject of a rather huge amount of experimental and theoretical work. A recent review was given by Ågren [3]. Using Synchrotron radiation it is possible to tune the photon energy into the various absorption states of the molecules. In Fig. 1 the different initial and final states for the three spectroscopical methods – photoionization, autoionization and Auger decay – are shown in a simple molecular orbital diagram. Whereas the photon induced transitions are governed by the dipole operator the radiationless decays after core to continuum and resonant excitation are governed by the coulomb operator. A better understanding of the observed processes deserves a calculation. Such calculations have already been applied to smaller molecules like CO [4], CO_2 [5], Ni–CO [6] and N_2O [7].

Benzene has been the subject of rather numerous spectroscopical and theoretical investigations ([8–12] and references therein).

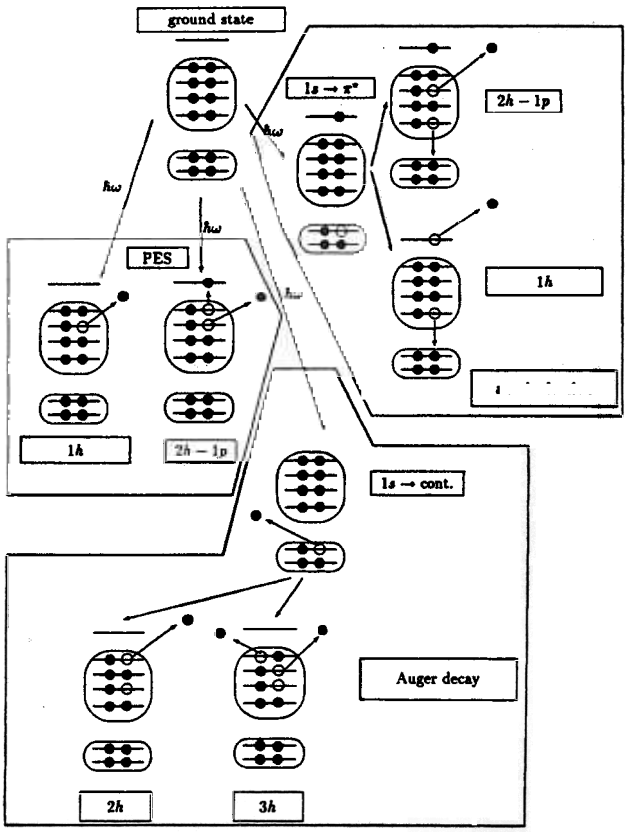

Fig. 1. Schematic representation of the numerous initial and final states in a simple molecular orbital diagram. For a discussion see text

In the present study we extend experimental and theoretical investigations to benzene as a prototype for large aromatic molecules. Isoelectronic molecules have recently been studied [13]. Additional insight into autoionization processes is gained by studying molecules of different symmetries [14].

2. Experimental details

The experiments have been performed at the Berlin storage ring for synchrotron radiation (BESSY) using the HE-TGM 2 monochromator [15]. The monochromator resolution at the C 1*s* ionization edge of condensed benzene was adjusted to 0.9 V. The photon energy of the monochromator was calibrated using the first π^* excitation of the condensed benzene as an energy reference of 285.5 eV [16, 17]. The near edge X-ray absorption fine structure (NEXAFS) at the C 1*s* edge (not shown) was recorded using a partial yield detector. This detector is described in Ref. [17]. The Cu(110) crystal surface was cleaned by repeated Ar ion sputtering and annealing cycles. Benzene was introduced via a leak valve. During exposure and measurement the crystal was held at 120 K. The thickness of the condensed film was estimated to correspond to 2–4 monolayers by controlling the total pressure during preparation. The emitted Auger- and photoelectrons were analyzed using a hemispherical energy analyzer with $\pm 1°$ angular acceptance and a position sensitive parallel detector (VSW). The measuring system is described in more detail elsewhere [18]. During the photoemission measurements the copper crystal surface was tilted 50° relative to the direction of the incident monochromatic synchrotron radiation. The electrons were collected normal to the sample surface.

3. Theoretical and computational considerations

The decay of a core hole excited state can proceed by autoionization or Auger processes. Exciting the system with a photon into a neutral state this state may decay radiationlessly via autoionization into the lower ion states of the system. Core to continuum excitation of the system by a photon yields a core ionized state which can decay radiationlessly via Auger decay into double ionized states. Within the *ab initio* Green's function formalism we calculate the autoionization as well as the Auger spectrum of benzene. The calculation of the autoionization and Auger spectrum is a three step procedure:

- Calculation of the photoelectron spectrum within the limit of sudden approximation.
- The resulting configuration interaction representation of the final ion state is used to calculate the autoionization spectrum after core to bound excitation.
- The results of the one-particle Green's function calculation is furthermore used to simulate the Auger spectrum.

It appears thus natural to divide the discussion of the simulation of the spectra into three sections.

3.1. *Calculation of the photoelectron spectrum*

Within the limit of sudden approximation the intensities measured in a photoelectron spectrum are governed by the following matrix elements:

$$I \propto |\langle \Psi_f | \boldsymbol{A} \cdot \boldsymbol{p} | \Psi_i \rangle|^2 \approx \left| \sum_k \langle \phi_f | \boldsymbol{A} \cdot \boldsymbol{p} | \phi_k \rangle \langle \Psi^n_{\text{ion}} | a_k \Psi_i \rangle \right|^2 \quad (1)$$

where Ψ_f and Ψ_i are initial and final states, respectively, Ψ^n_{ion} represents the nth final eigenstate of the ion. The ϕ_k and ϕ_f stand for the bound and continuum one-electron eigenstates, and a_k is the annihilitation operator of the kth electron. $\boldsymbol{A}$ and $\boldsymbol{p}$ are the vector potential of the photon field and the momentum operator, respectively. In the so-called sudden approximation for the final state $|\Psi^n_{\text{ion}}\rangle$ it is assumed that the removal of the photoelectron from the remaining N-1 electrons occurs fast, resulting in only negligible interaction between the two systems during ejection. Ionization energies and intensities are calculated in the present work via an *ab initio* Green's function method. The simulations of the spectra are based on *ab initio* self-consistent-field (SCF) calculations using an extended Gaussian basis set including polarization functions. The basis set consist of Gaussian functions: 9*s*/5*p*/1*d* on each carbon atom and four *s*-type functions and one *p* function on each H atom. This produces a total of 126 basis functions. The total SCF energy obtained with this basis set is $E_{\text{tot}} = -230.6684$ a.u. which is slightly lower than the best E_{tot} obtained for recent calculations: -230.5809 a.u. [10, 12]. However, E_{tot} is still slightly higher than the reported one by Ermler and Kern [39] of -230.7494 a.u. The SCF calculation has been performed with the vectorized Gaussian integral program MOLECULE of J. Almlöf [41]. In the one-particle Green's function calculation the third order

algebraic diagrammatic construction formalism ADC(3) [43] has been used to describe the valence ion states of benzene up to 30 eV binding energy within the limit of sudden approximation. For the expansion of the ionic-state wave functions, all single hole (h), single-particle (p), 2h1p and 2p1h configurations which arise in the given basis set are used. The orbitals have been slightly truncated in the third order calculation. A total number of 57 virtual orbitals have been taken into account and the core orbitals are neglected. The multiroot Davidson procedure [42, 44] is used to extract 50–80 solutions for each symmetry, where the dimension of the matrices is about 8700.

3.2. *Calculation of the autoionization spectrum*

We have used the ion state configuration interaction (CI) eigenvectors to calculate the transition probabilities for autoionization from the neutral highly excited state (a) to the valence ionized states (b) within the framework of Wentzel's ansatz [40]

$$I_{ab} \propto \sum_{l,m} |\langle \Psi^b_{\text{ion}} e^{(lm)} | \hat{H} | \Psi^a_{\text{neutral}} \rangle|^2 \tag{2}$$

Ψ^a_{neutral} represents the initial autoionizing state of the molecule, Ψ^b_{ion} is the final ion state, $\hat{H}$ and $e^{(lm)}$ are the Hamiltonian and the leaving electron, respectively. The initial state wave function is approximated by

$$|\Psi^a_{\text{neutral}}\rangle \approx |\phi_{\text{C } 1s \to 1e_{2u}}\rangle \tag{3}$$

i.e. a single determinant representation was chosen for the core to bound excited neutral state. The narrow π resonance in the near-edge-X-ray-absorption fine structure (NEXAFS) allows this conclusion to be drawn. For the final state wavefunction a configuration interaction wavefunction has to be used

$$|\Psi^b_{\text{ion}} e^{(lm)}\rangle \approx |\hat{A} \sum_{\mu} c_{\mu b} |\phi_\mu\rangle \psi_{lm} \tag{4}$$

where $\hat{A}$ represents the antisymmetrizer, ψ_{lm} are spherical waves centered at the core-hole site characterized by a set of angular momentum quantum numbers (l, m), describing the emitted electron. The ion state CI-eigenvectors have been taken from the calculation described above. Within this approximations the intensity is given as

$$I_{ab} = \sum_{l,m} \sum_{\mu,\nu} c^*_{\mu b} c_{\nu b} \langle \hat{A}\phi_\mu \psi_{lm} | \hat{H} | \phi_i \rangle \langle \phi_i | \hat{H} | \hat{A}\phi_\nu \psi_{lm} \rangle \tag{5}$$

using the abbreviation

$$M^{lm}_\nu = \langle \phi_i | \hat{H} | \hat{A}\phi_\nu \psi_{lm} \rangle \tag{6}$$

Equation (5) reduces to

$$I_{ab} = \sum_{l,m} \sum_{\mu,\nu} c^*_{\mu b} c_{\nu b} M^{lm*}_\mu M^{lm}_\nu \tag{7}$$

One has to differentiate four different types of valence ionized doublet final states under the assumption that the ground state of the molecule is a $^1\Sigma$ state. Without going into details for single hole states one obtains

$$M^{lm} = 2V_{1a\psi 1e_{2u}i} - V_{1s\psi i 1e_{2u}} \tag{8}$$

with the abbreviation

$$V_{1s\psi 1e_{2u}i} = \left\langle \phi_{1s}(1)\psi_{lm}(2) \left| \frac{1}{r_{12}} \right| \phi_{1e_{2u}}(1)\phi_i(2) \right\rangle \tag{9}$$

For 2h1p-configurations one has to calculate the following matrix elements M^{lm}.

- 2hp (singlet – coupled doublet): $(i<j)$

$$M^{lm} = \frac{1}{\sqrt{2}} (V_{1s\psi ij} + V_{1s\psi ji}) \tag{10}$$

- 2hp (triplet – coupled doublet): $(i<j)$

$$M^{lm} = \frac{\sqrt{3}}{\sqrt{2}} (V_{1s\psi ij} - V_{1s\psi ji}) \tag{11}$$

- 2hp both holes in the same spatial orbital: $(i = j)$

$$M^{lm} = V_{1s\psi ii} \tag{12}$$

The molecular orbitals ϕ_k are written as a linear combination of atomic orbitals (LCAO).

$$\phi_k = \sum_s c^k_s \chi_s \quad \text{with } k = i, j \tag{13}$$

Using the LCAO one can rewrite the remaining two electron integrals and evaluate them in the so called one-centre-approximation proposed by Siegbahn *et al.* [35] employing the radial integrals of McGuire [34]. The LCAO expansion coefficients have been taken from a SCF calculation with a STO-3G basis set in the equivalent core approximation. That means instead of taking the expansion coefficients of benzene the coefficients of the hypothetical molecule C_5H_6N in the experimental equilibrium geometry of benzene have been used. It has been shown experimentally [16] and numerically [4] that this localized picture is valid in case of core excitation. In doing so one completely neglects the vibronic coupling which has been shown to be sometimes of importance [5, 10, 16].

3.3. *Calculation of the Auger spectrum*

In the Green's function method employed here [32] the double ionization potentials (two-hole binding energies) are obtained as the negative of the poles of the particle–particle Green's function. The poles are the zeros of the eigenvalues of the inverse Green's matrix given by

$$\mathcal{G}^{-1}(\omega) = \mathcal{G}^{(0)-1}(\omega) - \mathcal{K} \tag{14}$$

where $\mathcal{K}$ is the irreducible vertex part with elements specified as follows:

$$\mathcal{K}^{(S,T)}_{klmn} = V_{klmn} \pm V_{klnm} \quad \text{if } k < l \text{ and } m < n$$

$$\mathcal{K}^{(S)}_{klmn} = V_{klmn} \quad \text{if } k = l \text{ and } m = n$$

$$\mathcal{K}^{(S)}_{klmn} = \sqrt{2}\, V_{klmn} \quad \text{if either } k = l \text{ or } m = n$$

V_{klmn} are the two-electron integrals and the upper/lower sign refers to singlets (S)/triplets (T) respectively.

Furthermore,

$$\mathcal{G}^{(0)}_{klmn}(\omega) = \sum_{i,j} \frac{F_{ki,lj} P_{ki} P_{lj} \delta_{km} \delta_{ln}}{(\omega - \omega_{ki} - \omega_{lj})} \tag{15}$$

where ω_{ki} are the poles of the one-particle Green's function and P_{ki} the corresponding pole strengths (k denotes the single-ionization species and i enumerates the possible solutions for this species). The factor $F_{ki,lj}$ equals -1 if k and l belong to the set of occupied orbitals, $+1$ if k and l belong to the set of virtual orbitals, and zero otherwise.

The transition rate $W_f^{(S,T)}$ to a final state $\Psi_f^{(S,T)}$ is estimated as

$$W_f^{(S,T)} = d^{(S,T)} \sum_{l,m} \sum_{iji'j'} M_{ij}^{(S,T)}(\psi_{lm})^* M_{i'j'}^{(S,T)}(\psi_{lm})^{Res} \omega_f(-\mathcal{G}_{iji'j'}^{(S,T)}) \tag{16}$$

where $d^{(S)} = 1$, $d^{(T)} = 3$ and $M_{i,j}^{(S,T)}$ is the matrix element of the electronic Hamiltonian between Hartree–Fock states where the initial state has a core hole and the final state has holes in orbitals ϕ_i, ϕ_j and an additional electron in a continuum orbital which is approximated by a spherical wave function ψ_{lm}, centered at the primary ionization site. The Auger matrix elements [3] are evaluated in the one-centre model [35] employing the radial integrals of McGuire [34] again. The expansion coefficients used for the evaluation of the transition rates are identical to the one described in the last section.

4. Results and discussion

4.1. *Experimental results*

In Fig. 2a comparison is shown between the C-*KVV* Auger spectrum of gaseous benzene recorded by Siegbahn *et al.* [19] and the C-*KVV* Auger spectrum of a condensed film of benzene molecules on a Cu(110) substrate. By Langmuir readings the film thickness of the disordered condensed molecular film is estimated to about 3 monolayers. Both spectra are referred to the kinetic energy scale. The reported Auger spectrum [20] of condensed benzene is equivalent to the one reported here. In the gas phase spectrum the first prominent Auger feature is found at 264.3 eV kinetic energy. The next structure at 262.2 eV is followed by the broad, intense main Auger feature of the benzene spectrum. The first two peaks and the onset of the main Auger contribution can be identified in the spectrum of the condensed phase although the structures are drastically broadened. This broadening is due to the decreased lifetime of the doubly ionized final states in the condensed phase. As indicated by the marks in Fig. 2 the structures in the spectrum of the condensed film are shifted by 2.4 eV to higher kinetic energy. This relaxation shift is due to extramolecular screening of the double ionized final state in the solid phase [20]. The C 1*s* near edge X-ray absorption yield of benzene can be found in the literature for gaseous benzene [21, 22] and for benzene adsorbed on various surfaces [16, 17, 23]. Studying the near edge structure by electron energy loss (EELS) a picture of the density of unoccupied molecular states in the presence of a core hole can be obtained. A recent assignment of structures in the yield spectrum of benzene has been given by Schwarz *et al.* [24]. The result can be transferred to the interpretation of X-ray absorption spectra, but differing from EELS measurements optical selection rules have to be applied in the interpretation of NEXAFS spectra [13, 25]. For condensed benzene an energy of 285.5 eV has been reported for the first π^* excitation [16]. A second resonance is found 3.7 eV above the first π^* excitation. From the calculations of Schwarz *et al.* [24] additional shake up configurations are expected at 3.7 eV above the first π^* resonance. For the benzene films studied here on a Cu(110) surface we have confirmed the same near edge structure as reported earlier for benzene on Ag(111) [17]. With these NEXAFS spectra we have calibrated the monochromator energy at 285.5 eV for the first π^* resonance of benzene on Cu(110).

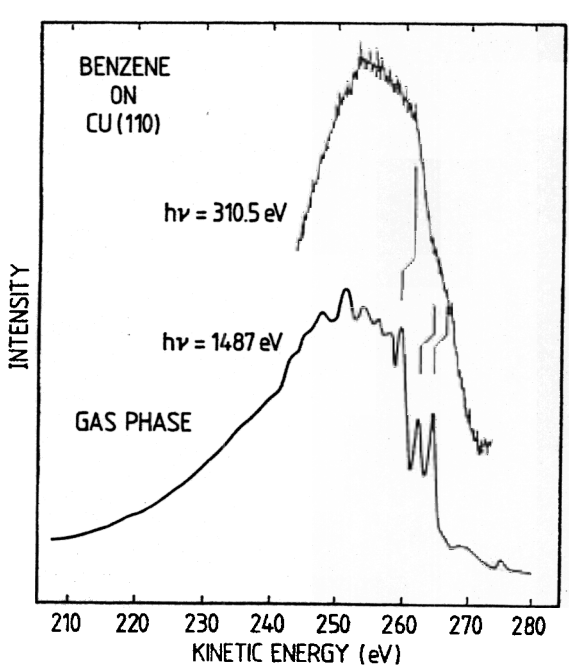

Fig. 2. Comparison between the C-*KVV* Auger spectrum of gaseous benzene recorded by Siegbahn *et al.* [19] and the C-*KVV* spectrum of a condensed film of benzene molecules on a Cu(110) substrate

Using synchrotron radiation one can tune into the various absorption states and thereby create different excited state electronic configurations, all involving a core hole at a carbon atom.

Figure 3 compares the Auger spectrum to the autoionization spectrum following the C $1s \rightarrow 1e_{2u}$ excitation populated by a photon energy of 285.5 eV. At this photon energy intense photoemission from copper d-bands occurs between 275 and 280 eV kinetic energy. These metallic states have no influence on the discussed molecular Auger transitions. Molecular states in the region at higher kinetic energy can better be observed in the difference curves of Fig. 4. At lower kinetic energies four structures are resolved.

In the deexcitation spectra of Fig. 3 an emission at 274 eV kinetic energy is partially superimposed by the intense Cu–*d* band emissions. Therefore in Fig. 4 two spectra are shown where the copper emissions have been subtracted using a photoionization spectrum excited with 280 eV photon-energy, 5 eV below resonance. In the difference curve the peak at 274 eV is clearly separated from the lower lying states. The binding energy $E_B = h\nu - E_{kin}$ of the 274 eV emission is only 11.5 eV and can thereby not be explained by a two hole final state configuration. We attribute this emission to an autoionization participator type process leading to a one hole final state. On the binding energy scale such states can be identified by comparison to photoemission spectra. Photoemission spectra of solid benzene can be found in the literature [36, 45]. The ionization potentials of benzene are collected in Table I relative to E_{vac} using a work function of the benzene copper system of 4.1 eV. The values in Table I compare well to those determined by Sesselmann [27] for benzene on Cu(110) and benzene adsorbed on Ag(111) [28]. From these values we can identify the peak at 11.5 eV binding energy to result from the $1a_{2u}$ lowest lying π orbital of benzene. The intense occurrence of the

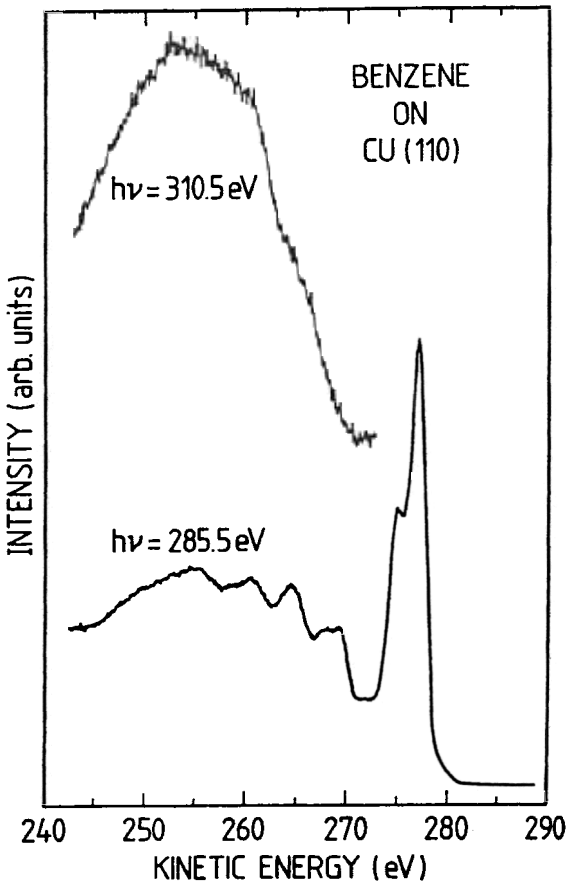

Fig. 3. The Auger spectrum of condensed benzene in comparison to the autoionization spectrum following resonant C $1s \rightarrow 1e_{2u}$ excitation populated by a photon energy of 285.5 eV

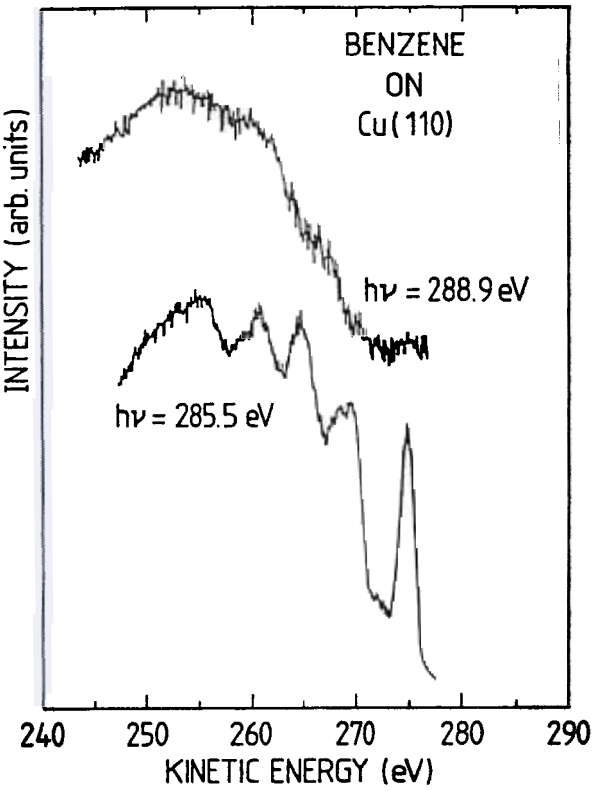

Fig. 4. Difference spectra of benzene after C 1*s*-to-bound excitation (bottom) and C 1*s*-to-continuum excitation (top). For the difference curve of the C 1*s*-to-bound excited spectrum a photoionization spectrum taken with a photon energy of $h\nu = 280.5$ eV has been subtracted from the raw data

lowest π orbital in the participator decay of the core hole has been observed also for the aromatic azabenzenes [13] and can be explained on the basis of *ab initio* Green's function calculations [14]. This exceptionally strong transition intensity can not be explained by the density of states in the vicinity of a carbon atom in the molecular ground state. As it will be shown the high intensity for the radiationless decay after core to bound excitation into single hole states of the form $1a_{2u}^{-1}$ is basically a result of the matrix elements by which these processes are governed.

4.2. *Computational results in comparison to the experiment*

The discussion of the computational results in comparison to the experiment is done in two steps: the first step concerns the assignment of the autoionization spectrum in comparison to the photoemission spectrum because both processes populate the same final ion states. The second step concerns the discussion of the Auger spectrum which populates double ionized valence states.

Figure 5 shows the results of the ADC(3) computations as a bar spectrum where degeneration of states has been taken into account. Only lines with a high single hole (1h) charac-

Table I. *Vertical binding energies of benzene in the gas and solid phase in comparison to the Koopman's energy [31] and the many particle corrected spectrum. All energies are given in eV*

	experimental		theoretical						
			this work		this work		condensed experimental		
Orbital			$-\varepsilon$		IP	P			this work
$1e_{1g}$	9.2	9.5	9.16	9.10	9.05	0.89	8.0	7.9	8.8 ± 0.5
$2e_{2g}$	11.5	12.0	13.46	11.95	12.07	0.90	11.9	10.5	11.2 ± 0.5
$1a_{2u}$	12.3		13.62	12.26	12.26	0.76			11.2 ± 0.5
$2e_{1u}$	14.0	14.0	15.97	14.46	14.35	0.87	13.1	(12.3)	13.2 ± 0.2
$1b_{2u}$	14.8	15.2	16.84	14.83	14.95	0.84		14.0	13.9 ± 0.3
$1b_{1u}$	15.5		17.43	15.75	15.66	0.84	14.0		14.7 ± 0.3
$2a_{1g}$	16.9		19.25	17.48	17.27	0.80	15.5		16.0 ± 0.2
$1e_{2g}$	19.1	19.0	22.30	20.01	19.53	0.36	17.7	17.7	18.0 ± 0.2
$1e_{1u}$	22.5	22.7	27.42		23.23	0.15		21.2	21.8 ± 0.2
$1a_{1g}$	26.0	25.7	31.09		26.44	0.13		24.5	25.1 ± 0.3

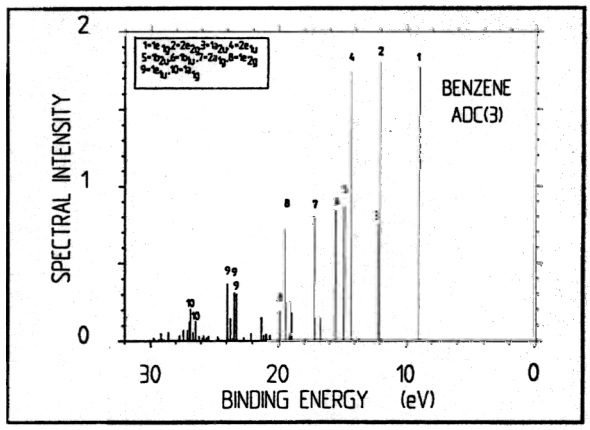

Fig. 5. Bar spectrum of the spectral intensity as a function of binding energy for gaseous benzene calculated by the ADC(3) method. For the plot degeneration has been taken into account. Only lines with a high single hole character are labeled

ter have been labelled. It is well accepted in the literature that the Green's function calculations show an overall satisfactory agreement between theory and experiment in case of photoionization [10, 12]. Whereas the $2e_{2g}$ and $1a_{2u}$ main lines coincide in the 2ph-TDA calculation [12] in this work the ordering of the main lines obtained confirms the results of a previous calculation [10] of the outer valence region. (Note: throughout this work we have numbered the molecular orbitals starting with the first valence orbital.) The total number of states obtained in the ADC(3) calculation is 464 up to 30 eV binding energy. About 73% of the states include a considerable amount of configurations with an excitation into the $1e_{2u}$ molecular orbital (LUMO) or exhibit a high single hole character. As outlined in the theoretical part these states have been used in the computation of the autoionization spectrum. In Figure 6 the bar spectrum of the autoionization lines is shown as a function of the binding energy. Intensities of degenerate states have been added up and only lines with an intensity $\geqslant 0.001$ (arb. units) have been drawn. The comparison of the computed photoemission (PES) Fig. 5 and autoionization spectrum Fig. 6 shows rather pronounced discrepancies over the whole energy range taken into account. States which exhibit a rather high spectral intensity in case of photoemission show almost negligible transition rates for the radiationless

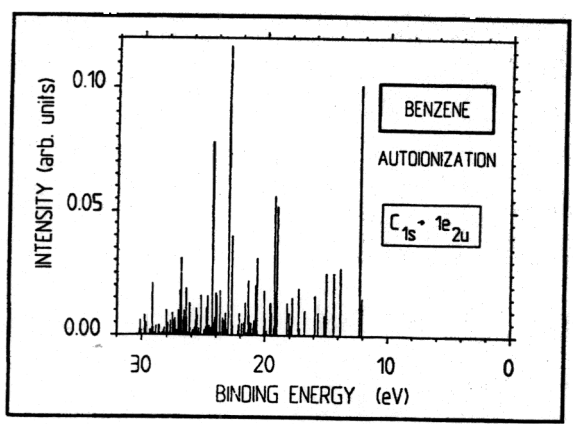

Fig. 6. Bar spectrum of the autoionization lines as a function of binding energy for gaseous benzene. Only lines with an intensity $\geqslant 0.001$ have been drawn. Intensities of degenerate states have been added up. For a detailed assignment of the states see Table II and text

decay. In the outer valence region up to 15 eV only one line clearly separates from the manifold of single hole states. In Table II we have collected the pole strengths and autoionization intensities after C $1s \rightarrow 1e_{2u}$ excitation of some states up to 20.9 eV binding energy along with the symmetry of the states in D_{2h} and D_{6h}. A full list of our results is available on request. The main configurations describing the states are given and only states which are important for the autoionization spectrum have been considered. From this table one identifies this state as having $^2A_{2u}$ symmetry. This pronounced feature in the spectrum is a result of the matrix elements by which the process is governed. Table III collects the intensities calculated assuming that one given configuration describes the state.

The pole strength of the main line of the $1a_{2u}$ MO is rather small for an outer valence orbital [12]. Correlation effects lead to an intense satellite line of A_{2u} symmetry at 16.78 eV ($P = 0.16$). However, this satellite has negligible intensity in case of autoionization. The regime of the single hole states shows rather small intensities besides the $^2A_{2u}$ band. This result is rather surprising due to the reason that at least five peaks with high single hole character are expected up to 15 eV binding energy. These are in particular the MOs $1e_{1g}$, $2e_{2g}$, $2e_{1u}$ and $1b_{2u}$ besides the $1a_{2u}$ orbital. The intensity for the radiationless decay into the highest occupied molecular orbital $1e_{1g}$ is small. The differences for the transition rates of the two π-orbitals ($1e_{1g}$ and $1a_{2u}$) can be found in the spatial distribution of the wavefunction and their overlap with the $1e_{2u}$ orbital.

In order to compare the computational results with the experiment we show the simulated bar spectrum as a Lorentzian convolution of the individual states taking a full width at half maximum (FWHM) of 2 eV over the entire energy range in Fig. 7. It should be mentioned that the heights of the bars below the curve differ from Fig. 6 due to the fact that the degenerate contributions have not been added up before drawing the lines. The experimental autoionization spectrum of benzene shows five resolved structures, due to the fact that our calculations are restricted to $\approx$30 eV binding energy we are not able to explain the peak at high binding energy. This does not imply that this peak cannot be assigned to autoionization final states but radiationless decay transitions between the core to bound excited neutral state and double ion outer valence states are likely to occur [33]. The overall agreement between theory and experiment is good. The four peaks resolved in the experimental spectrum up to 30 eV binding energy can be found in the theoretical curve. The maxima of the experimental resolved features correspond to the calculated ones. Only in the small interval of 13.8–15.0 eV binding energy the calculated transition rates seem to be over estimated. In this energy region three states of $^2E_{2u}$, $^2E_{1u}$, $^2B_{2u}$ have been calculated. In Fig. 8 the low energy part of the spectrum is shown in more detail and from inspection one gets the result that there is intensity in this energy region.

Several reasons might be the source for the minor deviation between the theoretical and experimental spectra in this energy region. The dominant source can be found in the fact that we are just considering the electronic part of the transition rates, neglecting vibronic coupling and lifetime effects in the initial and final states involved. It has been shown that benzene shows a complex vibrational structure

Table II. *Calculated ADC(3) ionization potentials (E_{IP}) (in eV), pole strengths (P) and autoionization intensities after C 1s → $1e_{2u}$ excitation of states up to 20.9 eV binding energy. Intensities and pole strength of degenerate states have been added up*

	P		Assignment of the main configurations[a]	State in D_{2h} $\sigma_h \to \sigma(xy)$ $\sigma_v \to \sigma(yz)$	D_{6h}
9.05	1.775	0.000	$1e_{1g}^{-1}$	$^2B_{3g} + {}^2B_{2g}$	$^2E_{1g}$
12.07	1.802	0.015	$2e_{2g}^{-1}$	$^2A_g + {}^2B_{1g}$	$^2E_{2g}$
12.26	0.748	0.101	$1a_{2u}^{-1}$, $(1e_{1g}^{-1}1e_{1g}^{-1}1e_{2u})^1$	$^2B_{1u}$	$^2A_{2u}$
13.81	0.017	0.027	$(1e_{1g}^{-2}1e_{2u})$, $(1e_{1g}^{-1}1e_{1g}^{-1}1e_{2u})^1$	$^2A_u + {}^2B_{1u}$	$^2E_{2u}$
14.35	1.740	0.025	$2e_{1u}^{-1}$, $(2e_{2g}^{-1}1e_{1g}^{-1}1e_{2u})^1$	$^2B_{2u} + {}^2B_{3u}$	$^2E_{1u}$
14.95	0.864	0.025	$1b_{2u}^{-1}$	$^2B_{3u}$	$^2B_{2u}$
15.12	0.000	0.008	$(1e_{1g}^{-2}1e_{2u})$, $(1e_{1g}^{-1}1e_{1g}^{-1}1e_{2u})^3$	$^2A_u + {}^2B_{1u}$	$^2E_{2u}$
15.66	0.842	0.009	$1b_{1u}^{-1}$	$^2B_{2u}$	$^2B_{1u}$
15.92	0.000	0.016	$(1e_{1g}^{-1}1e_{1g}^{-1}1e_{2u})^1$, $(1e_{1g}^{-2}1e_{2u})$	$^2A_u + {}^2B_{1u}$	$^2E_{2u}$
16.77	0.008	0.010	$(2e_{2g}^{-1}1e_{1g}^{-1}1e_{2u})^1$	$^2B_{3u} + {}^2B_{2u}$	$^2E_{1u}$
17.27	0.799	0.019	$2a_{1g}^{-1}$	^2A_g	$^2A_{1g}$
17.79	0.003	0.015	$(2e_{2g}^{-1}1e_{1g}^{-1}1e_{2u})^1$	$^2B_{2u} + {}^2B_{3u}$	$^2E_{1u}$
18.22	0.002	0.013	$(2e_{2g}^{-1}1e_{1g}^{-1}1e_{2u})^1$	$^2B_{3u} + {}^2B_{2u}$	$^2E_{1u}$
19.02	0.005	0.052	$(1a_{2u}^{-1}1e_{1g}^{-1}1e_{2u})^1$	$^2B_{3g}$	$^2B_{2g}$
19.03	0.177	0.019	$(2e_{1u}^{-1}1e_{1g}^{-1}1e_{2u})^1$	$^2B_{1g} + {}^2A_g$	$^2E_{2g}$
19.12	0.251	0.017	$(2e_{1u}^{-1}1e_{1g}^{-1}1e_{2u})^1$, $1e_{2g}^{-1}$	$^2B_{1g} + {}^2A_g$	$^2E_{2g}$
19.20	0.043	0.056	$(1a_{2u}^{-1}1e_{1g}^{-1}1e_{2u})^1$	$^2B_{2g} + {}^2B_{3g}$	$^2E_{1g}$
19.27	0.024	0.003	$(2e_{2g}^{-1}1e_{1g}^{-1}1e_{2u})^3$	$^2B_{2u} + {}^2B_{3u}$	$^2E_{1u}$
19.53	0.718	0.013	$1e_{2g}^{-1}$, $(2e_{1u}^{-1}1e_{1g}^{-1}1e_{2u})^1$	$^2B_{1g} + {}^2A_g$	$^2E_{2g}$
19.60	0.002	0.013	$(1a_{2u}^{-1}2e_{2g}^{-1}1e_{2u})^1$	^2A_g	$^2A_{1g}$
20.00	0.188	0.004	$1e_{2g}^{-1}$	$^2A_g + {}^2B_{1g}$	$^2E_{2g}$
20.03	0.000	0.018	$(1a_{2u}^{-1}1e_{1g}^{-1}1e_{2u})^3$	$^2B_{2g} + {}^2B_{3g}$	$^2E_{1g}$
20.07	0.013	0.004	$(1b_{2u}^{-1}1e_{1g}^{-1}1e_{2u})^1$	^2A_g	$^2A_{1g}$
20.61	0.019	0.002	$(2e_{1u}^{-1}1e_{1g}^{-1}1e_{2u})^3$	$^2A_g + {}^2B_{1g}$	$^2E_{2g}$
20.64	0.035	0.031	$(1b_{2u}^{-1}1e_{1g}^{-1}1e_{2u})^1$	$^2B_{1g} + {}^2A_g$	$^2E_{2g}$
20.76	0.000	0.020	$(1b_{2u}^{-1}1e_{1g}^{-1}1e_{2u})^1$	$^2B_{1g}$	$^2A_{2g}$
20.85	0.011	0.005	$(1b_{1u}^{-1}1e_{1g}^{-1}1e_{2u})^1$	^2A_g	$^2A_{1g}$

[a] The superscripts 1/3 refer to singlet/triplet coupled doublet states respectively. Configurations without a superscript are singlet coupled doublet states

in the C 1s → π* photoabsorption spectrum [16] confirming our interpretation.

Going to higher binding energies a lot of configurations start to mix making assignment difficult. In the energy range from 18–20 eV we have calculated about 20 states which show non negligible intensity contributions for the radiationless transition. The main contributions of those states are given by configurations of the form $(1a_{2u}^{-1}1e_{1g}^{-1}1e_{2u})^1$, $(2e_{2g}^{-1}1e_{1g}^{-1}1e_{2u})^1$, $(2e_{1u}^{-1}1e_{1g}^{-1}1e_{2u})^1$ and $1e_{2g}^{-1}$ where the superscript 1 refers to the singlet coupled doublet final state. In photoemission the main line of the $1e_{2g}$ MO is calculated at 19.5 eV (for experimental value see Table I). However, the strong experimental peak cannot be explained within the single particle picture. From Table III one derives again that the configurations involving the $1a_{2u}$ orbital are contributing most strongly to autoionization. We assign the second resolved peak at 19 eV in Fig. 7 to originate mainly from configuration of the type $(1a_{2u}^{-1}1e_{1g}^{-1}1e_{2u})^1$ with $^2B_{2g}$, $^2E_{1g}$ symmetry. These states are satellite states demonstrating once more that in the case of autoionization transition rates for 1h and 2h1p states may become equally sized. As it can be seen from the bar spectrum in Fig. 6 there are even more states contributing to the third resolved band in the spectrum. The assignment for this feature has to be rather tentative. Three states centred at 21.36 ($^2B_{1g}$), 22.98 ($^2E_{2u}$), 24.32 eV ($^2E_{1g}$) show very high transition rates. The leading configurations of these three states are $(1a_{2u}^{-1}1e_{1g}^{-1}1e_{2u})^1$, $(1a_{2u}^{-1}1e_{2u})^1$ and $(1a_{2u}^{-1}1e_{1g}^{-1}1e_{2u})^1$ respectively. However, these three states do not give full account for the spectral intensity contributing to the third resolved peak in the spectrum. This is due to the fact that ≈40 states are centred in the interval from 22–25 eV binding energy which show considerable transition rates. However, it is obvious that in this energy region the 2h1p configurations dominate the spectral features. The main lines calculated in case of photoionization in this energy region got $^2E_{2u}$ symmetry. Due to the different matrix elements which apply in case of autoionization a large amount of symmetries become allowed. The influence of triplet coupled doublet final states is increasing at higher binding energies but it can be seen from the matrix elements that the magnitude of the transition rates is rather low.

The assignment of the fourth resolved peak in the autoionization spectrum is even more difficult. As it can be seen from the calculated bar spectrum (Fig. 6) a huge amount of states contribute to this feature. As far as single hole states are concerned at 26.44, 26.86 and 27.09 eV states with high single hole character have been calculated. These

Table III. *Autoionization matrix elements due to pure configurations[a] after resonant C 1s → $1e_{2u}$ excitation. A total of 240 different configurations has been taken into account for the calculation of the transition rates*

Intensity	Configuration
0.009	$2e_{2g}^{-1}$
0.014	$2e_{1u}^{-1}$
0.092	$1a_{2u}^{-1}$
0.029	$1b_{2u}^{-1}$
0.011	$1b_{1u}^{-1}$
0.023	$2a_{1g}^{-1}$
0.002	$1e_{1g}^{-1}$
0.021	$1e_{2g}^{-1}$
0.021	$1e_{1u}^{-1}$
0.151	$1a_{1g}^{-1}$
0.027	$(1b_{2u}^{-2}1e_{2u})$
0.027	$(1b_{2u}^{-1}1e_{1g}^{-1}1e_{2u})^1$
0.008	$(2e_{1u}^{-2}1e_{2u})$
0.021	$(2e_{1u}^{-1}1e_{1g}^{-1}1e_{2u})^1$
0.101	$(1a_{2u}^{-2}1e_{2u})$
0.019	$(1a_{2u}^{-1}2e_{2g}^{-1}1e_{2u})^1$
0.083	$(1a_{2u}^{-1}1e_{1g}^{-1}1e_{2u})^1$
0.010	$(2e_{2g}^{-1}1e_{1g}^{-1}1e_{2u})^1$
0.034	$(1e_{1g}^{-2}1e_{2u})$

[a] The superscripts 1/3 refer to singlet/triplet coupled doublet states respectively. Configurations without a superscript are singlet coupled doublet states

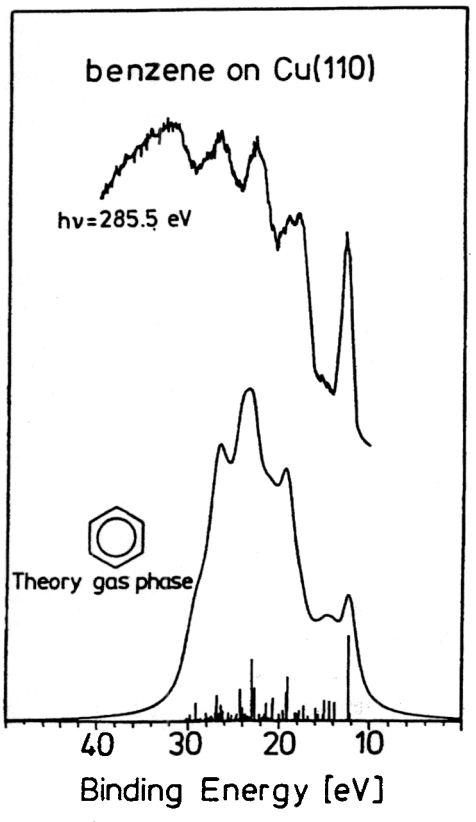

Fig. 7. Direct comparison between the calculated and measured autoionization spectrum of benzene after C 1s-to-bound excitation. The calculated autoionization spectrum is shown as the Lorentzian convolution of the transition rates of the individual states taking a constant FWHM of 2 eV over the entire energy range. As mentioned in the text only states up to ≈30 eV have been considered in the calculation of the autoionization spectrum

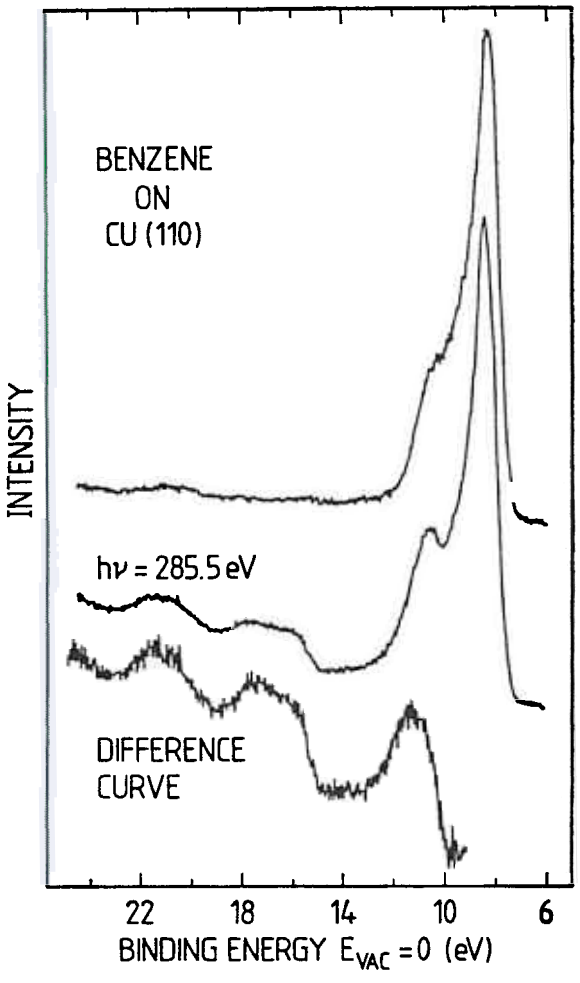

Fig. 8. Photoionization and autoionization spectrum of benzene after C 1s → $1e_{2u}$ excitation on the binding energy scale referenced to E_{vac}. The difference curve shows the autoionization features up to 24 eV binding energy in more detail

states got $^2A_{1g}$ symmetry but the 2h1p states with different symmetries dominate the spectrum. All lines are the result of many transitions having approximately equal weight and a description in terms of individual states is impossible.

Now we will turn to the discussion of the benzene spectrum after core to continuum excitation. In contrast to the autoionization spectrum in the Auger spectrum a core ionized state (see Fig. 1) is populated which undergoes radiationless decay into outer valence doubly ionized final states. Besides the charge and the spin multiplicity of the final state the configurations describing the individual states differ from the ones observed in autoionization spectra. As it has been shown [6] this concept even holds in the case of chemisorbed molecular adsorbates where the spectra after core to bound and core to continuum excitation got a similar overall shape [30]. In Fig. 4 the benzene spectra after core to bound and core to continuum excitation are shown on a common kinetic energy scale. At the bottom of the drawing the autoionization spectrum excited with a photon energy of 285.5 eV is shown. Just 3.4 eV above the π-resonance the spectrum changes drastically manifesting our interpretation. The simulated Auger spectrum of benzene is shown in Fig. 9 as a bar spectrum on the double ionization potential scale. A total number of 250 states has been calculated up to 53 eV double ionization potential where 133/117 states got singlet/triplet spin multiplicity

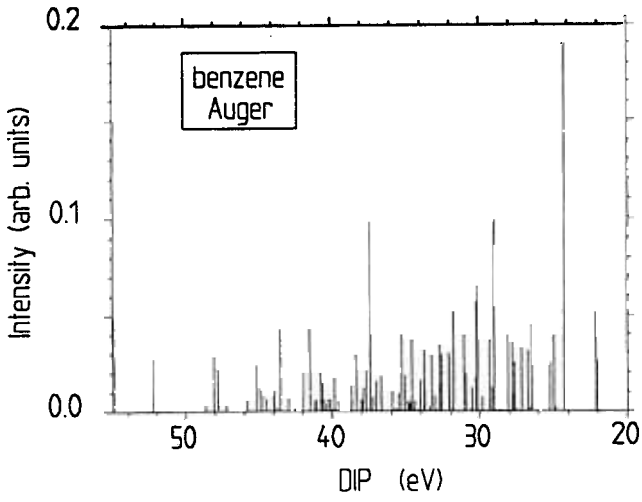

Fig. 9. Bar spectrum of the Auger lines as a function of the double ionization potential for gaseous benzene. Only lines with an intensity $\geqslant 0.001$ have been drawn. Intensities of degenerate states have been added up. For a detailed assignment of the states see Table IV and text

respectively. Great care has been taken in manifesting that the results obtained for the transition rates of the Auger spectrum are numerically stable. In particular we increased the number of configurations taken into account for the description of each individual line until the spectrum derived by the Lorentzian convolution of the bar spectrum did not change anymore. This is important due to the fact that only a few lines can be described by a small number of configurations. Already at low double ionization energy the familiar concept of a main state derived from a single 2h configuration is totally inapplicable. The majority of the states show substantial configuration mixing [11]. The lowest lying singlet/triplet state has been calculated at 22.04/21.61 eV double ionization energy respectively. For comparison the results for the lowest lying singlet/triplet state which have been calculated by Tarantelli *et al.* [11] are given by 23.96/23.34 eV respectively. In order to compare the theoretical results with experiment one has to convert the double ionization potential to the kinetic energy scale. The kinetic energy of the Auger electrons, assuming vertical transitions, is given by

$$E_{\text{kin}} = IP_c - DIP_v \tag{17}$$

where IP_c is a core ionization potential and DIP_v is a double ionization potential. The core ionization potential for benzene obtained by photoelectron spectroscopy is 290.3 eV [26, 46]. Taking this energy for the initial core ionized state in Fig. 10 we present our calculated bar spectrum as a Lorentzian convolution of the individual states assuming a constant FWHM of 2 eV over the entire energy range. The experimental gas phase [19] Auger spectrum and the spectrum obtained for the condensed phase are shown above the simulated curve. The overall agreement between the theoretical and experimental spectra is satisfactory. Comparing the calculated features at high kinetic energy with the intensities found for the gas phase spectrum, the computational features seem to be shifted to higher kinetic energies. The same result has been obtained by Tarantelli *et al.* [11]. In order to compare their results with experiment they have shifted all calculated states to lower kinetic energy so that the lowest calculated singlet state (DIP) coincides

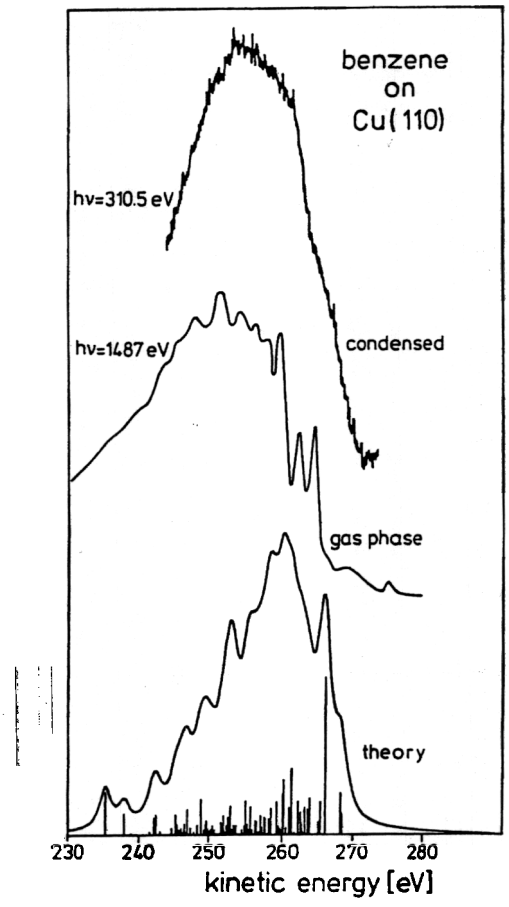

Fig. 10. Comparison between the calculated (bottom) and experimental (middle) Auger spectrum of gaseous benzene [19] and the Auger spectrum of condensed benzene (top) on the common kinetic energy scale. The calculated Auger spectrum is shown as the Lorentzian convolution of the transition rates of the individual states taking a constant FWHM of 2 eV over the entire energy range

with the first observed Auger peak. We did not adopt this procedure for several reasons. First of all in contrast to the calculations carried out by Tarantelli *et al.* [11] we have included the explicit calculation of the transition rates. One therefore expects to be able to give a more quantitative assignment of the spectrum. Comparing the gas phase spectrum with the theoretical curve shows that the eight resolved experimental features from 240 to 260 eV can be found in the simulated Auger spectrum. On the other hand, the overall shape of the Auger spectrum obtained for the condensed phase does not indicate that one has to shift the entire calculated spectrum.

In Table IV we have collected double ionization energies and calculated Auger intensities of some states. Only the leading configurations are given and intensities due to degenerate states have been added up. This table shows the complexity of the Auger spectrum. The assignment of the lowest double ionization potential states is compatible to the results obtained by Tarantelli *et al.* [11] and the main deviations result from the different selection of the states listed. The leading configurations up to 30 eV DIP include just the five outer valence molecular orbitals of benzene. Above this energy the inner valence orbitals show increasing importance. The singlet states dominate the spectrum whereas the transition rates into triplet states are rather low. We refer to Table III for matrix elements of pure components because the size of the Auger matrix elements is

Table IV. *Double ionization energies and calculated Auger intensities of some states. Only the leading configurations are given. Intensities due to degenerate states have been added up. All energies are given in eV*

Energy	I	main configurations	Energy	I	main configurations
22.04	0.026	$(1e_{1g}^{-2})$	30.96	0.019	$(1e_{2g}^{-1}1e_{1g}^{-1})^1$
22.17	0.052	$(1e_{1g}^{-2})$, $(1e_{1g}^{-1}1e_{1g}^{-1})^1$	31.10	0.040	$(1b_{2u}^{-1}1a_{2u}^{-1})^1$, $(1e_{2g}^{-1}1e_{1g}^{-1})^1$
24.27	0.190	$(1a_{2u}^{-1}1e_{1g}^{-1})^1$, $(1b_{2u}^{-1}2e_{2g}^{-1})^1$	31.82	0.053	$(1b_{2u}^{-1}2e_{2g}^{-1})^1$, $(2a_{1g}^{-1}2e_{2g}^{-1})^1$
24.85	0.002	$(2e_{2g}^{-1}1e_{1g}^{-1})^1$	31.85	0.032	$(2a_{1g}^{-1}1a_{2u}^{-1})^1$, $(1b_{1u}^{-2})$
24.95	0.040	$(2e_{2g}^{-1}1e_{1g}^{-1})^1$	31.96	0.001	$(1b_{1u}^{-1}2e_{1u}^{-1})^3$
25.20	0.025	$(2e_{2g}^{-1}1e_{1g}^{-1})^1$	32.12	0.028	$(2e_{1u}^{-2})$, $(2e_{1u}^{-1}2e_{1u}^{-1})^1$
26.48	0.045	$(1a_{2u}^{-2})$, $(2e_{2g}^{-2})$	32.17	0.030	$(2e_{1u}^{-2})$, $(1b_{1u}^{-2})$, $(2e_{1u}^{-2})$
26.60	0.002	$(2e_{1u}^{-1}1e_{1g}^{-1})^1$	32.63	0.029	$(2a_{1g}^{-1}2e_{2g}^{-1})^1$, $(1b_{2u}^{-1}2e_{2g}^{-1})^1$
26.61	0.001	$(2e_{1u}^{-1}1e_{1g}^{-1})^3$	32.78	0.035	$(1b_{1u}^{-1}2e_{2g}^{-1})^1$, $(1b_{2u}^{-1}2e_{1u}^{-1})^1$
26.76	0.031	$(2e_{1u}^{-1}1e_{1g}^{-1})^1$	32.99	0.001	$(1b_{2u}^{-1}2e_{1u}^{-1})^3$, $(1b_{1u}^{-1}2e_{2g}^{-1})^3$
27.19	0.033	$(2e_{1u}^{-1}1e_{1g}^{-1})^1$	33.13	0.008	$(1e_{2g}^{-1}2e_{2g}^{-1})^1$
27.57	0.001	$(1b_{1u}^{-1}1e_{1g}^{-1})^3$, $(2e_{1u}^{-1}1a_{2u}^{-1})^3$	33.34	0.029	$(1b_{2u}^{-1}2e_{1u}^{-1})^1$, $(1b_{1u}^{-1}2e_{2g}^{-1})^1$
27.67	0.025	$(1b_{1u}^{-1}1e_{1g}^{-1})^1$, $(2e_{1u}^{-1}1a_{2u}^{-1})^1$	33.44	0.002	$(1e_{2g}^{-1}1a_{2u}^{-1})^3$, $(2a_{1g}^{-1}2e_{2g}^{-1})^3$
27.74	0.008	$(2e_{2g}^{-2})$, $(2e_{2g}^{-1}2e_{2g}^{-1})^1$, $(2e_{1u}^{-1}2e_{1u}^{-1})^1$	33.81	0.011	$(1e_{2g}^{-1}2e_{2g}^{-1})^1$
27.82	0.036	$(1a_{2u}^{-1}2e_{2g}^{-1})^1$, $(1b_{2u}^{-1}1e_{1g}^{-1})^1$	33.84	0.032	$(1e_{2g}^{-1}1a_{2u}^{-1})^1$, $(2a_{1g}^{-1}2e_{2g}^{-1})^1$
28.13	0.040	$(2e_{2g}^{-2})$	34.07	0.016	$(1e_{2g}^{-1}2e_{2g}^{-1})^1$
28.67	0.001	$(2e_{1u}^{-1}1a_{2u}^{-1})^3$, $(1b_{1u}^{-1}1e_{1g}^{-1})^3$	34.17	0.001	$(1b_{1u}^{-1}1b_{2u}^{-1})^3$, $(1e_{2g}^{-1}2e_{1u}^{-1})^3$
29.04	0.099	$(1b_{2u}^{-1}1e_{1g}^{-1})^1$	34.43	0.005	$(1b_{1u}^{-1}1b_{2u}^{-1}$, $(1e_{2g}^{-1}2e_{1u}^{-1})^1$
29.19	0.012	$(1b_{1u}^{-1}1a_{2u}^{-1})^1$, $(2e_{1u}^{-1}2e_{2g}^{-1})^1$	34.60	0.004	$(1e_{1u}^{-1}1e_{1g}^{-1})^1$
29.34	0.038	$(2e_{1u}^{-1}1a_{2u}^{-1})^1$, $(1b_{1u}^{-1}2e_{2g}^{-1})^1$	34.66	0.038	$(2a_{1g}^{-1}2e_{1u}^{-1})^1$, $(1e_{2g}^{-1}1b_{1u}^{-1})^1$
29.82	0.007	$(2e_{1u}^{-1}2e_{2g}^{-1})^1$	34.72	0.006	$(2a_{1g}^{-1}1b_{1u}^{-1})^1$, $(1b_{1u}^{-1}1a_{2u}^{-1})^1$
30.18	0.066	$(1b_{2u}^{-1}1a_{2u}^{-1})^1$, $(1e_{2g}^{-1}1e_{1g}^{-1})^1$	34.74	0.002	$(1e_{1u}^{-1}1e_{1g}^{-1})^3$
30.18	0.001	$(1b_{1u}^{-1}1a_{2u}^{-1})^3$, $(2e_{1u}^{-1}2e_{2g}^{-1})^3$	34.84	0.004	$(1e_{1u}^{-1}1e_{1g}^{-1})^3$, $(2a_{1g}^{-1}1b_{1u}^{-1})^3$
30.27	0.057	$(2a_{1g}^{-1}1e_{1g}^{-1})^1$, $(1b_{2u}^{-1}2e_{2g}^{-1})^1$	34.87	0.003	$(1e_{1u}^{-1}1e_{1g}^{-1})^3$, $(2a_{1g}^{-1}1b_{1u}^{-1})^3$
30.31	0.017	$(1e_{2g}^{-1}1e_{1g}^{-1})^1$	34.94	0.005	$(1b_{1u}^{-1}1a_{2u}^{-1})^1$, $(2a_{1g}^{-1}1b_{1u}^{-1})^1$
30.54	0.001	$(1e_{2g}^{-1}1e_{1g}^{-1})^3$	35.10	0.018	$(1e_{1u}^{-1}1e_{1g}^{-1})^1$
30.55	0.012	$(2e_{1u}^{-1}2e_{2g}^{-1})^1$	35.13	0.014	$(1b_{1u}^{-1}2e_{1u}^{-1})^1$, $(2a_{1g}^{-1}2e_{2g}^{-1})^1$
30.64	0.001	$(1e_{2g}^{-1}1e_{1g}^{-1})^3$	35.32	0.041	$(1b_{2u}^{-2})$, $(1e_{2g}^{-1}2e_{2g}^{-1})^1$

proportional to the ones listed for autoionization processes. One major difference can be found in the assignment of the Auger and autoionization spectra. In the autoionization spectrum the lowest lying π orbital ($1a_{2u}$) is playing a dominant role. However, in the double ionized final states the influence of the $1a_{2u}$ orbital decreases. On the double ionization energy scale the three lowest states are described by configuration of the type $1e_{1g}^{-1}$, $1a_{2u}^{-1}1e_{1g}^{-1}$ and $1b_{2u}^{-1}2e_{2g}^{-1}$. The first two peaks are derived from emission out of the highest occupied molecular π orbital $1e_{1g}$. This orbital shows a large influence up to 31 eV. All outer valence orbitals couple to the highest occupied π-orbital. Above 31 eV double ionization potential the inner valence orbitals show increasing influence. In the kinetic energy interval 261–259 eV 12 states with considerable transition rates have been calculated. The majority of the configurations describing the states are characterized as $(1e_{1g}^{-1}i^{-1})$ and $(1e_{2g}^{-1}i^{-1})$ where i denotes an outer valuence molecular orbital. It can be noted from Table IV that lines involving the $1b_{2u}$, $1a_{2u}$ and $2a_{1g}$ orbitals show the largest intensities. This is not surprising because this basically represents the spatial localization of the ion states involved. However, as can be seen from Table IV it is rather impossible to assign a certain feature in the experimental spectrum to a few configurations because the density of states is rather high and configuration interaction plays a dominant role.

It should be mentioned that our calculations include a large amount of configurations involving the three inner most valence orbitals ($1e_{2g}$, $1e_{1u}$ and $1a_{1g}$). These orbitals are almost totally missing in the ADC(2) calculations carried out by Tarantelli *et al.* [11]. The influence of the three inner most orbitals can already be noted at low energies (Table IV) and above 38 eV (DIP) they dominate the spectral features.

5. Conclusions

Auger and autoionization spectra of condensed multilayers of benzene on Cu(110) have been presented.

In order to interpret, analyse and assign the spectra of benzene we have carried out Green's function calculations on *ab initio* level of the photoionization, Auger and autoionization spectrum.

The comparison to the experimental results prove that the theoretical concept described in this work gives a useful quantitative assignment of the photoelectron spectra obtained in case of core excitation.

- The reported results show that the radiationless decay after core to bound and core to continuum excitation populate different final states.
- Core to bound excitation leaves the molecule in a highly excited neutral state which decays radiationless into outer valence ion states. Whereas the initial state for the Auger decay is a core ionized state which decays radiationless into outer valence double ionized states.

- It has been shown that the $1a_{2u}$ MO, the lowest lying π-orbital of benzene plays a dominant role in the autoionization processes.

Acknowledgements

The assistance of N. Schwarz and J. Krieger in connection with data transfer is gratefully acknowledged. The present work was financially supported in part by the "Bundesministerium für Forschung und Technologie" under project 05 432 FAB 0. We thank K.-H. Frank and F. Netzer for their support of the measurements. H.-J. F. thanks the Fonds der Chemischen Industrie for support. G. D. thanks the Hertz Stiftung for a scholarship.

References

1. Hanson, D. M., Advan. Chem. Phys. **77**, 1 (1990).
2. Freund, H.-J. and Neumann, M., Appl. Phys. **A47**, 3 (1988).
3. Ågren, H., Int. J. Quantum Chem. **39**, 455 (1991).
4. Freund, H.-J. and Liegener, C.-M., Chem. Phys. Lett. **134**, 70 (1987).
5. Porwol, T., Illing, G., Freund, H.-J., Kuhlenbeck, H., Neumann, M., Bernstorff, S., Braun, W., von Niessen, W. and Liegener, C.-M., Phys. Rev. **B41**, 10510 (1990).
6. Porwol, T., Dömötör, G., Hemmerich, I., Illing, G., Freund, H.-J. and Liegener, C.-M., Verhandl. DPG(VI) **26**, O15.2 (1991).
7. Larkins, F. P., Eberhardt, W., Lyo, J. W., Murphy, R. and Plummer, E. W., J. Chem. Phys. **88**, 2948 (1988).
8. Hutson, F. L. and Ramaker, D. E., J. Chem. Phys. **87**, 6824 (1987).
9. Siegbahn, H. and Karlsson, L., in: "Handbuch der Physik, Photoelectron Spectroscopy" (Edited by W. Mehlhorn) (Springer, Berlin 1982), Vol. 31.
10. von Niessen, W., Cederbaum, L. S. and Kraemer, W. P., J. Chem. Phys. **65**, 1378 (1976).
11. Tarantelli, F., Sgamelotti, A., Cederbaum, L. S. and Schirmer, J., J. Chem. Phys. **86**, 2201 (1987).
12. Cederbaum, L. S., Domcke, W., Schirmer, J., von Niessen, W., Diercksen, G. H. F. and Kraemer, W. P., J. Chem. Phys. **69**, 1591 (1978).
13. Dudde, R., Rocco, M. L. M., Koch, E. E., Bernstorff, S. and Eberhardt, W., J. Chem. Phys. **91**, 20 (1989).
14. Porwol, T., Dömötör, G., Freund, H.-J., Liegener, C.-M. and von Niessen, W., to be published.
15. Bernstorff, S., Braun, W., Mast, M., Peatman, W. and Schroeter, T., Rev. Sci. Instrum. **60**, 2097 (1989).
16. Ma, Y., Sette, F., Meigs, G., Modesti, S. and Chen, C. T., Phys. Rev. Lett. **63**, 2044 (1989).
17. Yannoulis, P., Dudde, R., Frank, K. H. and Koch, E. E., Surf. Sci. **189/190**, 519 (1987).
18. Dudde, R., Frank, K. H., Rocco, M. L. and Koch, E. E., Surf. Sci. **201**, 469 (1988).
19. Siegbahn, K., Nordling, C., Johanson, G., Heckmann, J., Heden, P. F., Hamrin, K., Gelius, U., Bergmann, T., Werme, Lo. O., Manne, R. and Baer, Y., in: "ESCA Applied to Free Molecules" (North Holland, Amsterdam 1969).
20. Rogers, J. W., Houston, J. E. and Rye, R. R., Surf. Sci. **141**, L345 (1984).
21. Eberhardt, W., Haelbich, R. P., Iwan, M., Koch, E. E. and Kunz, C., Chem. Phys. Lett. **40**, 180 (1976).
22. Hitchcock, A. P., Pocock, M., Brion, C. E., Banna, M. S., Frost, D. C., McDowell, C. A. and Wallbank, B., J. Electr. Spectr. Rel. Phen. **13**, 345 (1978); Hitchcock, A. P. and Brion, C. E., J. Electr. Spectr. Rel. Phen. **10**, 317 (1977).
23. Horsley, J. A., Stöhr, J., Hitchcock, A. P., Newbury, D. C., Johnson, A. L. and Sette, F., J. Chem. Phys. **83**, 6099 (1985); Johnson, A. L., Muetterties, E. L. and Stöhr, J., J. Am. Chem. Soc. **105**, 7183 (1983); Johnson, A. L., Ph. D. Thesis, University of California (1986).
24. Schwarz, W. H. E., Chang, T. C., Seeger, U. and Hwang, K. H., Chem. Phys. **117**, 73 (1987).
25. Sommers, J., Robinson, A. W., Lindner, Th., Ricken, D. and Bradshaw, A. M., Phys. Rev. **B40**, 2053 (1989).
26. Gelius, U., Basilier, E., Svensson, S., Bergmark, T. and Siegbahn, K., J. Electr. Spectr. Rel. Phen. **2**, 405 (1974).
27. Sesselmann, W., Ph. D. Thesis, Universität München (1983).
28. Dudde, R., Frank, K. H. and Koch, E. E., Surf. Sci. **225**, 267 (1990).
29. Chen, C. T., Di Dio, R. A., Ford, W. K., Plummer, E. W. and Eberhardt, W., Phys. Rev. **B32**, 8434 (1985).
30. Menzel, D., Feulner, P., Treichler, R., Umbach, E. and Wurth, W., Phys. Scr. **T17**, 166 (1987).
31. Koopmans, T., Physica **1**, 104 (1932/1933).
32. Liegener, C.-M., Chem. Phys. Lett. **90**, 188 (1982); Chem. Phys. **92**, 97 (1985); Chem. Phys. Lett. **106**, 201 (1984).
33. Illing, G., Porwol, T., Hemmerich, I., Dömötör, G., Kuhlenbeck, H., Freund, H.-J., Liegener, C.-M. and von Niessen, W., J. Electr. Spectr. Rel. Phen. **51**, 149 (1990).
34. McGuire, E. J., Phys. Rev. **185**, 1 (1969); Sandia Laboratories Research Report SC-RR-69-137 (1969) (unpublished).
35. Siegbahn, H., Asplund, L. and Kelfve, P., Chem. Phys. Lett. **35**, 330 (1975).
36. Riga, J., Pireaux, J. J., Caudano, R. and Verbist, J. J., Phys. Scr. **16**, 346 (1977).
37. Lunnell, S., Svensson, S., Malmquist, P.-A., Gelius, U., Basilier, E. and Siegbahn, K., Chem. Phys. Lett. **54**, 420 (1978)
38. Grobman, W. D., Koch, E. E. and Karlsson, L., in: "Photoemission in Solids II" (Edited by L. Ley and M. Cardona) (Springer, Berlin, Heidelberg, New York 1979).
39. Ermler, W. C. and Kern, C. W., J. Chem. Phys. **58**, 3458 (1973).
40. Wentzel, G., Z. Physik **43**, 524 (1927).
41. Almlöf, J., MOLECULE, Vectorized Gaussian Integral Program, University of Lund, Sweden (1986).
42. Davidson, E. R., J. Computational Phys. **17**, 87 (1975); Liu, B., NRCC Report No. LBL 8158 (1978) (unpublished).
43. Schirmer, J., Cederbaum, L. S. and Walther, O., Phys. Rev. **A28**, 1237 (1983).
44. Tarantelli, F. (private communication). In the calculations we used a program of Tarantelli, F.
45. Freund, H.-J., in: "Electronic Structure of Solids: Photoemission Spectra and Related Data" (Edited by Landolt–Börnstein), New Series III, Vol. 23a, p. 162–278; "Condensed Molecules" (Edited by A. Goldmann and E. E. Koch) (1989).
46. Spohr, R., Bergmark, T., Magnusson, N., Werme, L. O., Nordling, C. and Siegbahn, K., Phys. Scr. **2**, 31 (1970).